



Combining X-ray micro-CT and microscopy-based images of two lianas species to derive structural, mechanical and functional relationships

Claudine Karlen¹ · Pascal Turberg^{1,2,3} · Alexandre Buttler^{1,2} · Océane Martin³ · Fritz Schweingruber⁴ · Anastasios P. Vassilopoulos⁵

Received: 16 March 2023 / Accepted: 7 January 2024
© The Author(s) 2024

Abstract

This paper presents a biomechanical study of stems of two liana species, *Clematis vitalba* and *Vitis vinifera*, investigates the mechanical performance of these two liana species and attempts to enhance the understanding of structure–function relationships. The investigation involved mechanical testing of whole plant stems, supplemented by X-ray micro-CT (X-ray computed tomography at micron voxel size) imaging and 2D microscopic images of stained cross sections of the plant stems, to derive structure–function relationships with potential for application in bioinspired composite materials. The micro-CT images were compared to the microscopic images of stained cross sections, in order to show benefits and potential drawbacks of the X-ray micro-CT method with respect to traditional methods. The high-resolution 3D imaging capacity of micro-CT is exploited to explain the structural functionality derived from the mechanical testing. A simple finite element model is developed based on the plant topology derived by the micro-CT images and proved accurate enough to model the plant's mechanical behaviour and assess the influence of their structural differences. The two plants exhibit different to each other physical and mechanical properties (density, strength and stiffness) due to their common growth form. Anatomical cross-sectional observation and X-ray micro-CT provide complementary information. The first method allows the identification of the lignified parts, supposedly more resistant mechanically, of these structures, while the second one provides a full 3D model of the structure, admittedly less detailed but providing the spatial distribution of density contrasts supposed to be important in the mechanical properties of the plant. The proposed methodological approach opens new perspectives to better understand the mechanical behaviour of the complex structure of plants and to draw inspiration from it in structural engineering.

Keywords Histology · Liana · Plant mechanics · Plant structure · X-ray micro-CT

Introduction

To use natural structures for inspiring development of technical structures (biomimetics) involves a detailed understanding of structure–function relationships in nature and

the creation of an abstracted model of the natural principle to be used in a technical application.

In the field of lightweight construction and materials, great interest of research lies on fibre reinforced composites inspired by plants. The goal in such efforts is to develop structures with efficient resource use and optimal mechanical properties (Masselter and Speck 2011). The link between

Handling Editor: Julius Jeiter.

✉ Anastasios P. Vassilopoulos
anastasios.vassilopoulos@epfl.ch

¹ School of Architecture, Civil and Environmental Engineering ENAC, Laboratory of Ecological Systems ECOS and Plant Ecology Research Laboratory PERL, École Polytechnique Fédérale de Lausanne EPFL, 1015 Lausanne, Switzerland

² Swiss Federal Institute for Forest, Snow and Landscape Research WSL, Site Lausanne, 1015 Lausanne, Switzerland

³ School of Architecture, Civil and Environmental Engineering ENAC, École Polytechnique Fédérale de Lausanne EPFL, PIXE Platform, 1015 Lausanne, Switzerland

⁴ Swiss Federal Institute for Forest, Snow and Landscape Research WSL, 8903 Birmensdorf, Switzerland

⁵ School of Architecture, Civil and Environmental Engineering ENAC, Composite Construction Laboratory CCLab, École Polytechnique Fédérale de Lausanne EPFL, 1015 Lausanne, Switzerland

composites and plants lies in the fibre-matrix composition inherent to both structures, as well as in the structural organization in plants on several hierarchical levels that presents a great potential when transferred to composites (Baley et al. 2018; Masselter and Speck 2011). An example of such biomimetic engineering is the “technical plant stem”, developed by the German “Competence Network Biomimetics” project (Competence Network Biomimetics—Technical plant stem). This technical fibre composite material is the result of the translation and combination of seven different structural functionalities of the stems of two plant species, Dutch rush (*Equisetum hyemale*) and giant reed (*Arundo donax*), leading to outstanding lightweight properties and high compression and bending stiffness (Milwich et al. 2006).

Underlying such engineering success is the science of plant biomechanics, that searches to explain the relation between plant anatomy and morphology, and their mechanical functionalities (Niklas et al. 2006), and to derive specific mechanical implications of the structural properties. Such studies commonly aim at comparing different species (Hoffmann et al. 2003; Isnard et al. 2003; Kaack et al. 2003), growth forms (self-supporting and non-self-supporting) (Isnard et al. 2003) and ontogenetic stages (corresponding to old stages of development with significant secondary growth) (Hoffmann et al. 2003; Isnard et al. 2003; Rowe et al. 2004). Further, a particular mechanical behaviour is often being related to the environmental conditions prevailing in the respective plant habitat (Ennos 1993; Isnard et al. 2003).

In biomechanical research, technical methods for characterizing mechanical properties and for imaging natural structures are key to understand structure–function relationships. Mechanical properties such as the modulus of elasticity can be determined with bending (Dixon et al. 2015; Hoffmann et al. 2003; Isnard et al. 2003; Kaack et al. 2003; Obataya et al. 2007), tensile (Baley et al. 2018) torsion (Hoffmann et al. 2003) or compression tests (Obataya et al. 2007), testing either a whole stem segment or separate samples of different tissue types (Rüggeberg et al. 2008).

Morphological properties of the plants can be measured directly on the sample or by using microscopic images of stem cross sections, whereby they can be evaluated with help of imaging softwares (Baley et al. 2018; Dixon et al. 2015; Jellum 1962; Kaack et al. 2003; Niklas et al. 2006; Obataya et al. 2007; Rüggeberg et al. 2008). However, for imaging the complex internal structure of plants at high resolution, the technique of X-ray microcomputed tomography (X-ray micro-CT) has increasingly received attention as it can produce a three-dimensional imaging of the variations of material density (tomodensitometry) at micron voxel size which makes it possible to determine primarily the 3D structure of the plant’s voids but also to identify the major variations in density throughout the organic material of the plant in a

non-destructive way as presented for example in Holmlund et al. (2019), Mylo et al. (2021), Toumpanaki et al. (2021) and, with a specialized X-ray instrument (XRM) that incorporates microscope objective lenses in Duncan et al. (2022). In addition, X-ray micro-CT can be applied to any type of plant, its measurement can be repeated on the same sample if necessary and, as the measurement is non-destructive, the same sample can be used for other tests at a later date (e.g. mechanical tests). It thereby represents a time-saving and functionally identical laboratory based alternative to traditional techniques involving sectioning and light microscopy (Brodersen and Roddy 2016; Mayo et al. 2010). The generated images serve for qualitative and quantitative analysis, and are increasingly being used as an input for finite element (FE) modelling of structural properties (Maire and Withers 2014). In the application to plants, micro-CT has the potential for qualitative and quantitative analysis of wood microstructures (Calo et al. 2020; Mayo et al. 2010; Moshtaghin et al. 2016) for studying plant hydraulics through analysis of xylem structure (Brodersen et al. 2013; Brodersen and Roddy 2016; Gao et al. 2020; Koddenberg and Militz 2018; Li et al. 2020) and for understanding physiological processes in plants (Pajor et al. 2013). In addition, micro-CT can be used to image structural developments over time (4D monitoring) (Maire and Withers 2014; Pajor et al. 2013).

Industrial and biomimetic considerations have motivated the use of micro-CT in plants to study the mechanical behaviour of plant tissues. For example, micro-CT-based FE analysis has been applied to scan maize stalks in order to estimate the properties with special lodging resistance (Von Forell et al. 2015). Interest also lies on bamboo as a material with great biomimetic and industrial potential. Dixon et al. (2018) built 3D printed models of bamboo parenchyma tissue for mechanical testing based on micro-CT images. Palombini et al. (2016, 2019) have published several works on micro-CT-based FEA of the mechanical behaviour of bamboo parenchyma and sclerenchyma tissue. They focused on the comparison of different discretizing methods in FEA, having identified the transfer of image data to a discretized mesh as a critical step in the methodology, due to the difficulty of preserving the detailed structure at the cellular level and of attributing the appropriate mechanical properties to the structure (Palombini et al. 2020). However, to the authors knowledge, micro-CT has never been assessed in its benefits and drawbacks compared to traditional imaging of plant material, nor in its potential for facilitating biomimetic research. Therefore, this study presents an assessment of micro-CT to better understand structure–function relationships of plants while critically comparing the potential of micro-CT with that of a traditional imaging method.

This paper presents a comparative biomechanical study of stems of two liana species, *Clematis vitalba* and *Vitis vinifera*. The two plants exhibit particular mechanical

properties due to their growth form. The investigation involved mechanical testing of the plant stems, supplemented with X-ray micro-CT imaging and 2D microscopic images of stained cross sections of the plant stems, to derive structure–function relationships and to point out benefits and potential drawbacks of the micro-CT method with respect to traditional cross-sectional methods. Finally, the results of a simple finite element mechanical model based on the plant topology derived from the micro-CT images were compared to the results of the mechanical tests to demonstrate the consistency in the differential behaviour of the two tested lianas. The aim of this study is to demonstrate the differential mechanical behaviour of two plant species that are closely related, due to their specific microstructures. More generally, it also aims to demonstrate the widespread potential of micro-CT to provide a coherent structural model for quantitative functional analysis of plants. Through a better understanding of this structure–function relationship, this study enables us to consider plants even more accurately as a source of biomimetic inspiration for designing future engineering materials and structures.

Materials and methods

Plant material

Clematis vitalba and *V. vinifera* were chosen in this research as two liana species expected to show remarkable climbing mechanical properties and occurring in similar habitats at low altitude and in temperate climate in Switzerland. The two species exhibit a few differences in their internal structures (e.g. periderm and phloem geometry, vessel dimensions and spatial distribution, pith diameter), despite the similar growth form, which was regarded as meaningful for comparison and analysis of structure–function relationships. Conversely to many other woody perennial crops, the *Vitis vinifera* grapevine does not display self-supporting and limited-in-space aerial architectures, but rather develops extended shoot systems relying on external mechanical supports (Torregrosa et al. 2021). This behaviour results from both structural factors, *i.e.* stem anatomy, bud and phytomer organization, and also specificities in the modulation of primary growth and branching. *Clematis* is a cosmopolitan genus of the Ranunculaceae showing a range of growth forms mostly confined to perennial herbs and climbers among its 250 species. Woody aerial plant stems are extremely rare in the Ranunculaceae and seldom, if ever, show self-supporting characteristics (Isnard et al. 2003). Growth form evolution in the group may have been canalized by evolution of rhizomatous geophytic growth forms with secondary growth confined to underground stems (Liu et al. 2016). Certain body plan organizations appear to have

inbuilt mechanical constraints which may have profound effects on the subsequent evolution of growth forms. *Vitis* is inferred to have originated in the New World during the late Eocene (39.4 Ma), then migrated to Eurasia in the late Eocene (37.3 Ma) (Liu et al. 2016) while the stem age of the Vitaceae family was proposed to be around 90.7 Ma (Wen et al. 2013). Ranunculaceae became differentiated in forests and buttercup crown group was estimated around 109 Ma (Wang et al. 2016) and *Clematis* (Clematidaceae) around 29 Ma (He et al. 2022). *Clematis vitalba* was sampled at the margin of a riverine forest, climbing on a poplar tree (Cudrefin, VD, 46°58'4"–7°2'12") and *V. vinifera* could be found as an old unpruned plant of “chasselas” grape variety climbing on bushes in an abandoned vineyard (Boudry, NE, 46°56'52"–6°51'3"). Stems of different diameters of *C. vitalba* and *V. vinifera* were sampled on living plants and stored immediately in a conditioning room with a constant temperature of 20 °C and a relative humidity of 65% (between 1 and 3 months) and dried to approximately constant weight, before being imaged by CT and by anatomical cross sections and mechanically tested. Diameters of *C. vitalba* stems ranged from 5.6 to 18.5 mm, and those of *V. vinifera* ranged from 4.6 to 13.0 mm.

Anatomical cross sections

For the anatomical description, a stem of *C. vitalba* corresponding to old stages of development with significant secondary growth (stage 4 according to Isnard et al. (2003), Schweingruber (1983)) was used (diameter of 16 mm). For *V. vinifera*, a stem of 13 mm was used, corresponding to an old stem of several years. Sectioning for microscopic analyses was performed with a sledge microtome which enabled sectioning without prior embedding of the stems. The sections were stained directly on a glass slide for several minutes with a 1:1 solution of Astrablue and Safranin. Lignified cell walls are stained red from Safranin, and non-lignified structures are stained blue from Astrablue. Subsequently, the sections were dehydrated with 96% ethanol, anhydrous ethanol and xylene, embedded in Canada balsam and covered with a cover glass. The followed procedure is described in more detail in Gärtner and Schweingruber (2013). Photographs of the cross sections were taken in normal light with an Olympus BX51 Microscope.

X-ray microcomputed tomography

Similar-sized stems as for the anatomical cross section were used for the micro-CT analyses. Each of the plant stem sections was scanned with an X-ray micro-CT Ultratom scanner from RX-Solutions (Fig. 1) and with the same parameters. A Hamamatsu high power X-ray generator was used, in reflexion mode, with a 0.2 mm thick copper filter and a tungsten

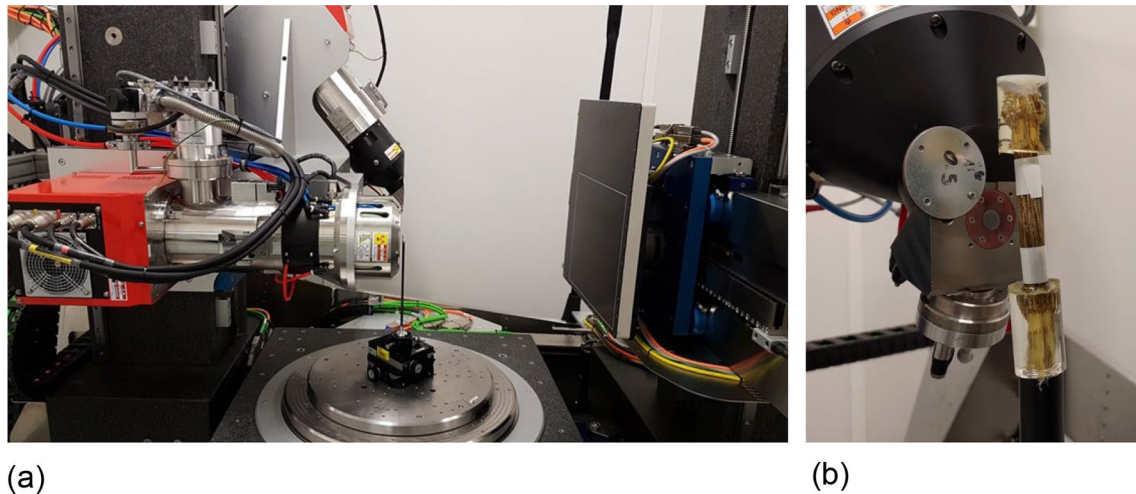


Fig. 1 **a** General view of the Ultratom scanner system with its two X-ray generators showing the turn table supporting the sample and the plane detector. **b** Zoom on the sample of a *Vitis vinifera* sample mounted for measurement at the high power microfocus X-ray generator

target. The acquisition was performed in cone beam mode with a current of 150–170 μA and a voltage of 50–60 kV. During data acquisition, the plant sample was rotated by 360 degrees and 1632 projections were taken by steps of 0.22° to ensure a precise volume reconstruction. The X-ray beam attenuation was registered by an XL Varian 2530 plane detector with 2176×1792 pixels. The projections were then processed (X-act RX-Solutions, Filtered Backprojection) to reconstruct a corrected volume composed of some hundreds of slices in 16bit Tiff format (typically between 800 and 1500 slices). According to the sample, the cubic voxel edges length is between 7 and 9 microns.

Image analysis

Micro-CT images were processed with AVIZO (Thermo Fisher Scientific, v-2019.2). First, raw images were filtered (non-local means filter) then segmented by intensity thresholding to best differentiate the three major components of the plant that were visually identified on the CT images and to best correspond to the main structures identified on the histological thin slices: (a) the high attenuation regions representing the high-density material of the plant (HD) with grey values over 26,500 for Clematis and over 33,500 for Vitis, (b) the intermediate attenuation regions (ID) with grey values between 23,160 and 26,500 for Clematis and between 28,500 and 33,500 for Vitis and (c) the low attenuation regions which represent the voids of the plant (V) with grey values under 23,160 for Clematis and under 28,500 for Vitis. As expected, due to the grey values contrast, the delimitation of the threshold between HD and ID material was more difficult than the delimitation of the threshold between the latter two regions and the voids V, which exhibit a clear

attenuation contrast. An additional criterion for determining by visual inspection the thresholds was that the voids and wood materials were globally not over- or underestimated. Then, the volumes of the three segmented components (HD, ID and V) were calculated for each plant (on a representative volume of about 460 slices) as well as the contribution in volume per cent of these components to the total volume of the plant sample.

Mechanical tests

Sample preparation

Stems adjacent to those used for CT measurements and for anatomical thin sections were used to test mechanical properties of the two lianas. Sections of the stems of *C. vitalba* and *V. vinifera* were prepared, comprising a node on either extremity of the sample to facilitate fixation. The length of samples of *C. vitalba* ranged from 10 to 20 cm, with diameters from 5.6 to 18.5 mm. The length of samples of *V. vinifera* ranged from 8 to 15 cm with diameters from 4.6 to 12.7 mm. Due to the curvature of some branches and the short internode distances, a minimum sample length of ten times its diameter, as required for tensile testing, could not be guaranteed in all samples. For fixation in the testing machine, both ends of a sample (including the nodes) were embedded in plastic tubes filled with resin. Epofix resin and hardener (Sicommin Epoxy-Härter, Suter-Kunststoffe AG) were used and mixed at a 25:3 weight ratio. Epofix resin has a pot time of ca. 30 min and cures after ca. 8 h at 20°C . Prior to embedding, any barks were removed from the sample extremities and adherence between wood and resin was improved by either carving the extremities in contact with

the resin or adding staples to the wood. The specimens were left drying for at least 12 h. Finally, two parallel surfaces on either fixation tube were sanded, enabling proper fixation of the specimens in the traction machine. Characteristic specimens of both plant species and a detail showing the trimmed gripping area are shown in Fig. 2. Overall, twenty-five *C. vitalba* and twenty *V. vinifera* specimens were tested in order to obtain a significant set of valid experimental data.

Tensile experiments

Tensile experiments on most of the specimens were carried out on a 5 kN electromechanical Walter + Bai testing machine under displacement-control mode at a rate of 1 mm/min at controlled temperature of 22 ± 3 °C. The machine was equipped with two external linear variable differential transformer (LVDT) deformation sensors with accuracy of ± 0.02 mm for the measurement of the deformation. The tensile experiments on specimens of *C. vitalba* with a diameter greater than 13 mm were performed by using a Walter + Bai 250 kN hydraulic testing device. In that case, the axial deformation was measured by a video extensometry system composed of a 10-bit Sony XCLU1000 CCD connected to a Fujinon HF35SA-1 lens, with a focal length of 35-mm and an aperture, f 1.4–22, able to provide an accuracy of ± 0.005 mm. In both cases, the axial stresses were calculated using the load recorded by the machine's load cell and the initial cross-sectional area. The testing set-up/equipment used in this investigation is presented in Fig. 3.

Numerical modelling

A finite element analysis was successfully performed on both *C. vitalba* and *V. vinifera* plants to model their mechanical behaviour under tension. In order to simplify the plant modelling, it has been decided to extrude only one section of the plants' stem, and therefore, the FE model would have a uniform plant cross section along the plant axis. The tiff images extracted from the micro-CT were treated with an intensity threshold, segmenting the section into two parts for (a) the high-density attenuation regions (HD, as defined in section “[image analysis](#)”) and the intermediate attenuation regions (ID, as defined in section “[image analysis](#)”) were merged to compose the plain section of the plant, and (b) a low attenuation region (V) composing the voids of the plant. Representative sections from specimens C6 and V4 for *C. vitalba* and *V. vinifera*, respectively, are selected for this simulation and shown in Fig. 4. The stem of the *C. vitalba* was 85.1 mm long and had a 9.3 mm diameter. The area of the section including voids is 67.9 mm^2 and without the voids is 49.2 mm^2 . The stem of the *V. vinifera* was 58 mm long, had a radius of 6 mm, an area with voids of 113.1 mm^2 and without voids 91.8 mm^2 .

Tiff images of Fig. 4 were used as a basis to draw dxf sketches with smoother edges in order to diminish the number of vertices for easier meshing. Considering the symmetry axis of both plants, only a quarter of the *C. vitalba* section was drawn while a half of the *V. vinifera* section

Fig. 2 Characteristic specimens of both species. Top: C16 specimen, diameter 11.6 mm. Middle: V20, *Vitis vinifera* specimen, diameter 10.9 mm. Bottom: sanded surface for fixation



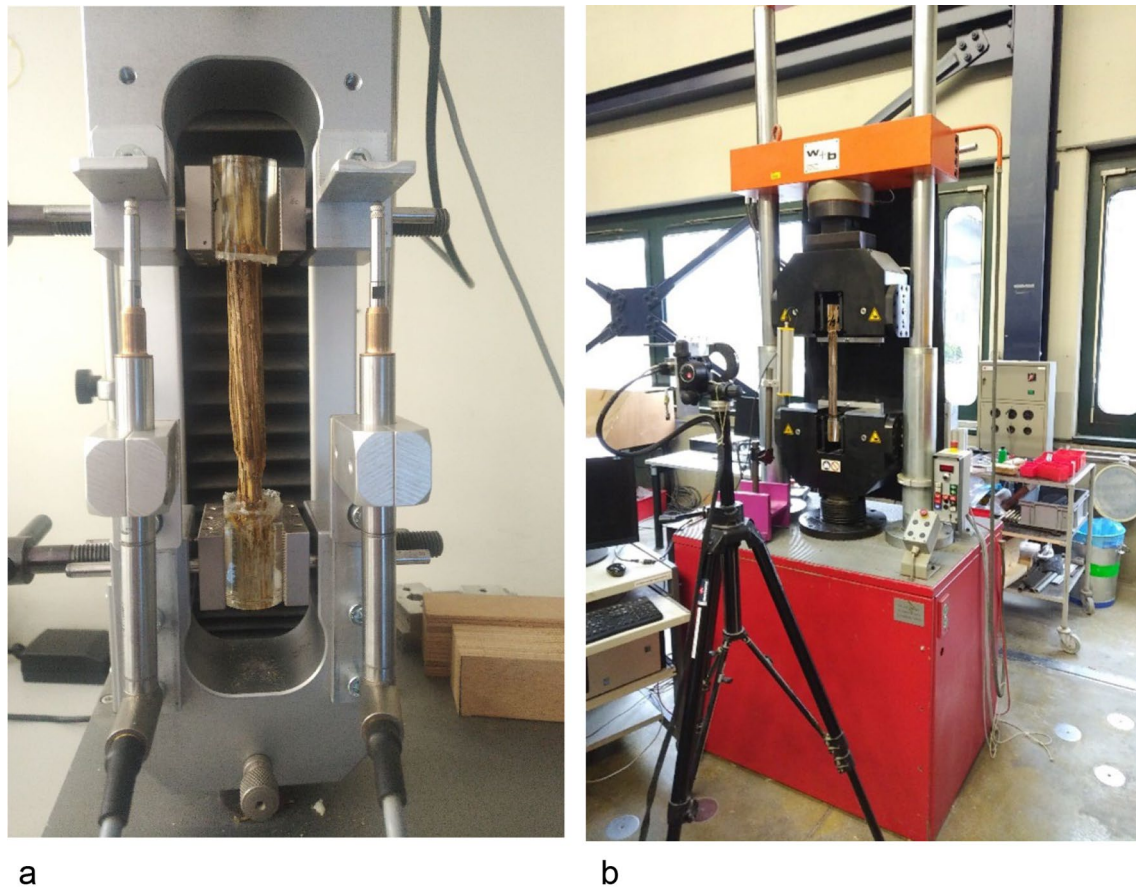


Fig. 3 Experimental set-up for tensile tests. 5 kN machine (a), 250 kN machine (b)

was necessary. Although this oversimplifies the plant cross section (that is not symmetric due to the natural growth of the plants), it seems like a reasonable and practical approach since the model will be used in the future for introducing, symmetric in principle, biomimetic structures. Both drawings are shown in Fig. 5.

The FE analysis software ABAQUS 6.14-1 under academic license was used to perform the simulations. Mechanical properties of both plants were derived from mechanical testing, by only keeping the successful mechanical tension tests. The plants' material was assumed elastic isotropic with an elastic modulus of 1200 MPa for *C. vitalba* and 2170 MPa for *V. vinifera* (see next section). The Poisson's ratio equals to 0.45 for both plant species, assumed similar to common soft wood species properties as given in Green et al. (1999).

These stiffness values were selected based on the experimental evidence for the two plant species under investigation. However, it is known that plants' properties are subjected to change with age. The phenomenon is called ontogenesis to describe the development of an individual organism or an anatomical feature from an earlier stage to

maturity. For example, the self-supporting plant group, of which bamboo is part, presents significant increase in the Young modulus in bending during its lifetime while the non-self-supporting lianas, such as the *C. vitalba* and *V. vinifera*, present a significant decrease of the Young modulus during their lifespan (Speck and Burgert 2011).

Results

Anatomical characterization

Figure 6 shows microscope images of the anatomical cross sections of *C. vitalba* and *V. vinifera*, stained with Astrablue and Safranin. These selected samples had a diameter of 16 mm and 13 mm (in the direction of the longer axis of the oval) for *C. vitalba* and *V. vinifera*, respectively. In *C. vitalba* (Fig. 6a), we can distinguish the open collateral vascular bundles in circular alignment around the pith, separated by the medullary rays of parenchymatic tissue. Parenchyma cells consist of thin primary cell walls that can either

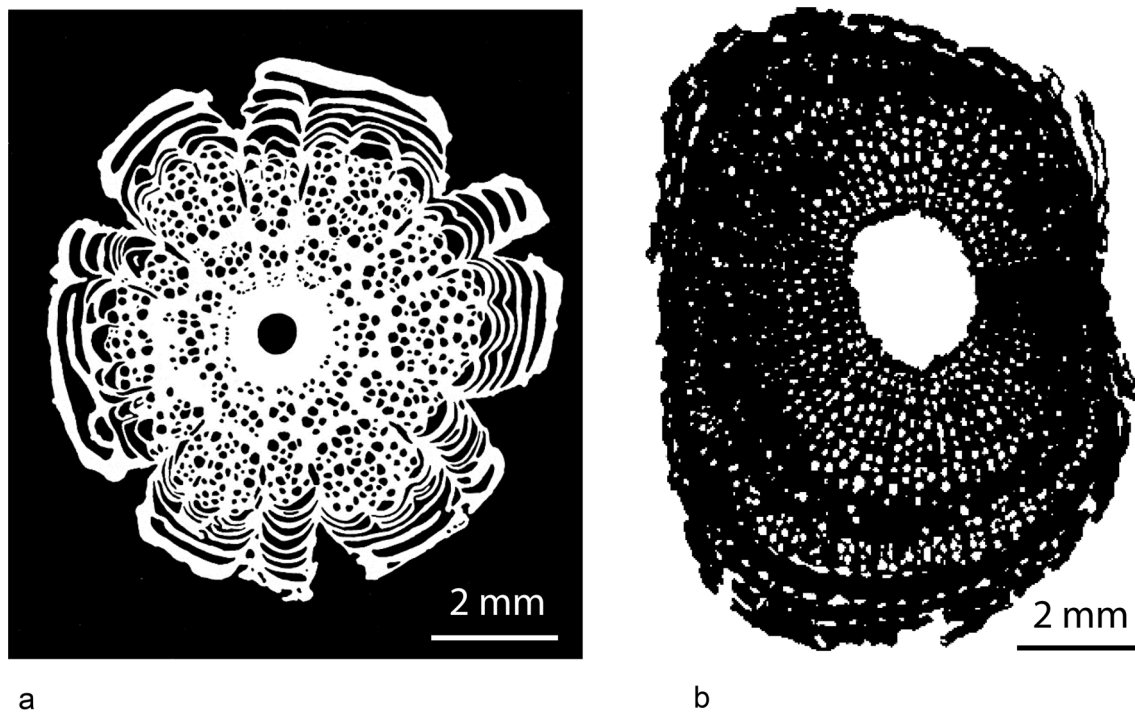


Fig. 4 Processed tiff images (Binarized plant stems sections) of plants' cross section for the FEA simulations (**a** *Clematis vitalba*, **b** *Vitis vinifera*)

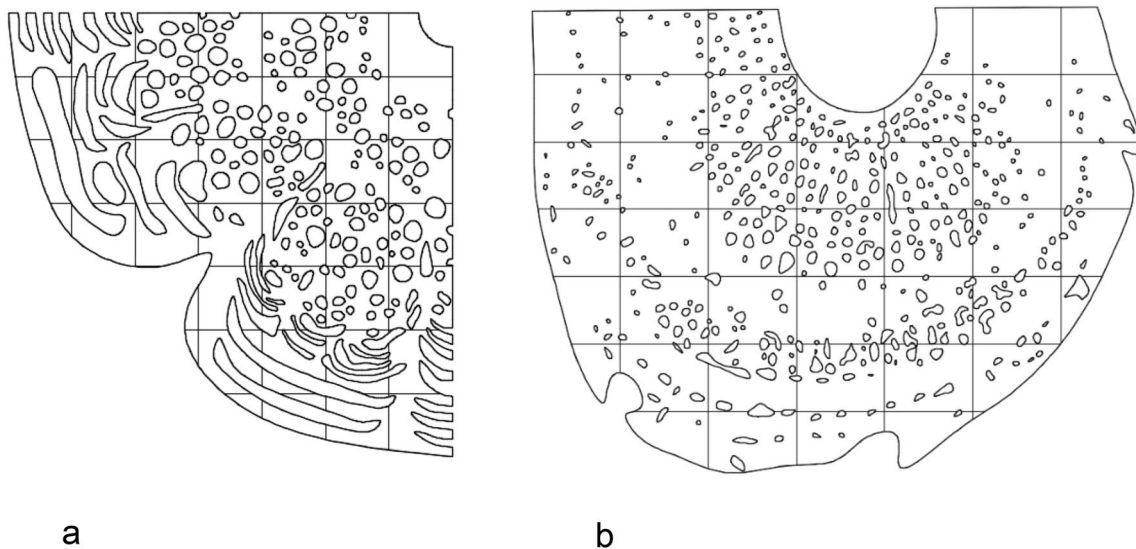


Fig. 5 Sketches of plants' cross section for the FEA simulations (**a** *Clematis vitalba*, **b** *Vitis vinifera*)

be lignified or non-lignified and their function is to store nutrients (Lehmann and Schulz 1976; Schweingruber and Börner 2018). Figure 6 also shows a clear difference in the radial organization of xylem vessels, which are very present towards the periphery in *C. vitalba* (Fig. 6a) and much less so in *V. vinifera* (Fig. 6v).

The ray parenchyma in *C. vitalba* is lignified (red). The vascular bundles comprise the xylem and the phloem. The

xylem consists of vessels (large cells, to conduct water) and fibres. Fibres are made of sclerenchyma cells which are dead and have thick lignified secondary cell walls, and provide the main structural support of the plant. Vessels also consist of dead cells with lignified secondary cell walls, which also contribute to the stability of plant. The phloem is made of living, non-lignified (blue) cells (sieve elements) that serve for the conduction of assimilates, and fibres (red) for

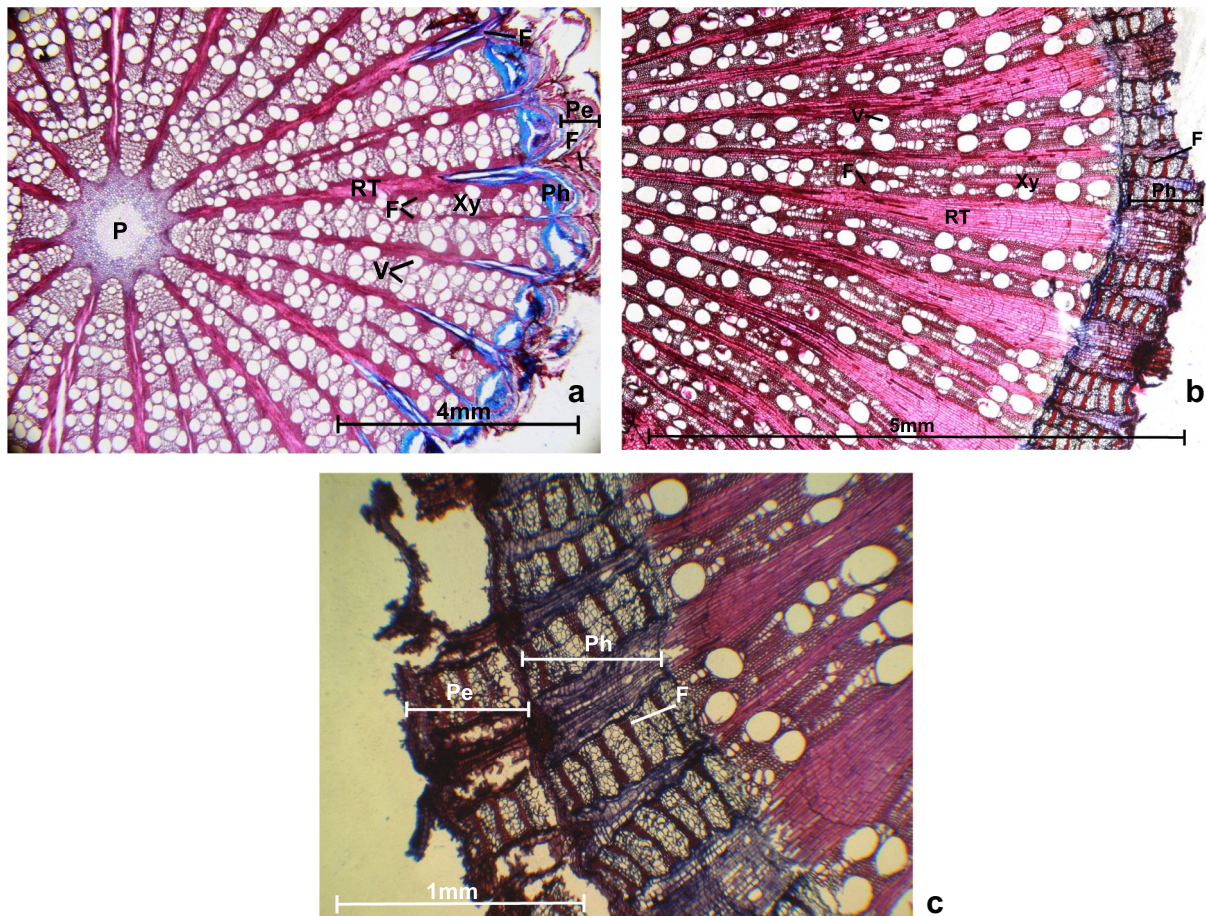


Fig. 6 Anatomical cross sections of the stem of *C. vitalba* (a) and *V. vinifera* (b and c) Red and blue colours represent lignified and non-lignified tissue, respectively. *P* pith, *RT* ray tissue (parenchyma), *Xy* xylem, *Ph* phloem, *Pe* periderm, *V* vessels, *F* fibres (sclerenchyma)

support. The periderm, or bark, represents the outermost layer. The structure of *V. vinifera* is similar (Fig. 6b), with open collateral vascular bundles separated by the medullary rays and, at the outer layer, a small phloem, reinforced with fibres, while the periderm is missing on this section. Figure 6c shows a zoomed in view where the periderm is present. When comparing the structures of the two species, we notice that the xylem in *V. vinifera* exhibits proportionally fewer vessels, thus less void, and more fibre cells than in *C. vitalba*.

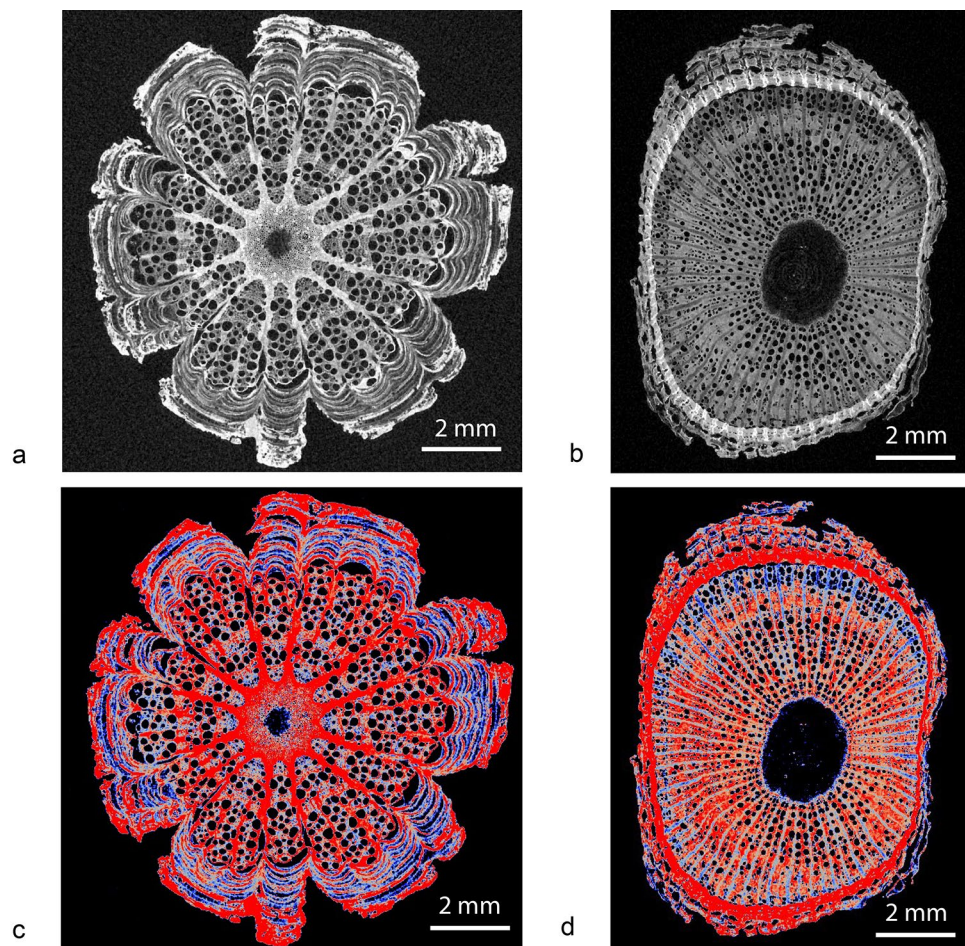
CT analysis of microstructures

The micro-CT structures of *C. vitalba* and *V. vinifera* are presented in 2D with grey values (Fig. 7, top) in a transverse section relative to the stem axis of the plant. The coloured representation according to the image intensity grey values of these slices, chosen to highlight the internal structure as clearly as possible, is shown in Fig. 7 (bottom) for both plants and can be compared to the anatomical thin sections as presented in Fig. 6. One can observe that the cross section

of the stem of *C. vitalba* (left) shows a regular circular shape with a small central void, whereas the cross section of *V. vinifera* exhibits a slightly oval shape with a larger void, which is not exactly located in the centre of the section. According to the image intensity, in *C. vitalba*, the high-density material is concentrated in the medullary rays, in the fibres enclosing the phloem and in the periderm. In *V. vinifera*, the medullary rays are of relative lower density material but the in between xylem is of high-density material. Importantly, one can distinguish an outer ring (the phloem) of intense red colour, indicating a high density of the organic material. On the direct inside of this ring, a distinct layer of xylem with low density (blue) is visible. The high contrast in grey values between the vessels and the plant material of both lianas tend to confirm that the vessels were mostly desaturated.

Figure 8 shows 3D micro-CT-based representations of *C. vitalba* (top) and *V. vinifera* (bottom), in raw grey values (left) and after colouring according to image intensity in the same way as shown in Fig. 7 (right). The images reveal that the 2D structures which can be observed in Fig. 7 are repeated equally in the axial direction without any helicoidal

Fig. 7 Micro-CT transverse slices of *Clematis vitalba* (a) and *Vitis vinifera* (b); in grey values. *Clematis vitalba* (c) and *V. vinifera* (d), in a coloured representation of the same sections using a continuous colour scale for easy comparison with the histological sections in Fig. 6. Red colour represents regions of relative high density, blue colour represents regions of relative intermediate density and black colour represents regions of relatively low density (voids)



effect. Also, when considering the volumes of the three material components (HD, ID and V), as shown in the profiles of volume fractions of Fig. 9, only negligible variations of the material components in the axial direction can be noted. Further, these results reveal that in *C. vitalba*, the intermediate density material ID presents in average the largest volume fraction (53%), followed by the high-density HD material (26.4%) and the voids (20.6%). In *V. vinifera*, the high-density material accounts for the highest volume fraction (61.7%) and the low-density material (19.0%) as well as the voids (19.3%) make up a similar, small fraction.

Figure 10 shows a 3D representation of the voids (essentially vessels) alone in the two species. *Clematis vitalba* exhibits relatively large voids that are regularly distributed around the central pith. In *V. vinifera*, the vessel size decreases towards the outside of the stem (in a radial direction), except for the outermost layer of xylem of lower density. Furthermore, the asymmetry of the voids is visible, the voids to the left and right side of the pith (as shown in Fig. 7) being larger than those on the top and bottom of the pith. A similar spatial distribution of vessels in *V. vinifera* was observed in the work of Brodersen et al. (2013).

As the CT measurements were carried out on two specimens of similar size with identical measurement parameters, the quantification of structures between *C. vitalba* and *V. vinifera* is based on almost similar image resolutions (voxel size between 7 and 9 microns) and can reasonably be assumed to involve relatively comparable objects.

Mechanical properties

Typical failure modes of both specimen types are presented in Fig. 11. Due to their natural growth, most of the specimens were not completely straight, while their irregular cross section was not entirely circular. In some cases, short internode distances did not allow to have long enough specimens without a node in the free length, or very close to the free length in the gripping part (Fig. 11d). Due to this inconsistent geometry and material distribution of the specimens, no prevailing failure mode could be identified. As shown in Fig. 11, specimens C1 (Fig. 11a), C2 (Fig. 11b), C10 (Fig. 11c) and V19 (Fig. 11f) failed at the free length, with C10 specimen showing a split failure. V7 specimen (Fig. 11d) failed at a node close to the gripping areas and V14 (11e) failed at the borders of the gripping area. Most

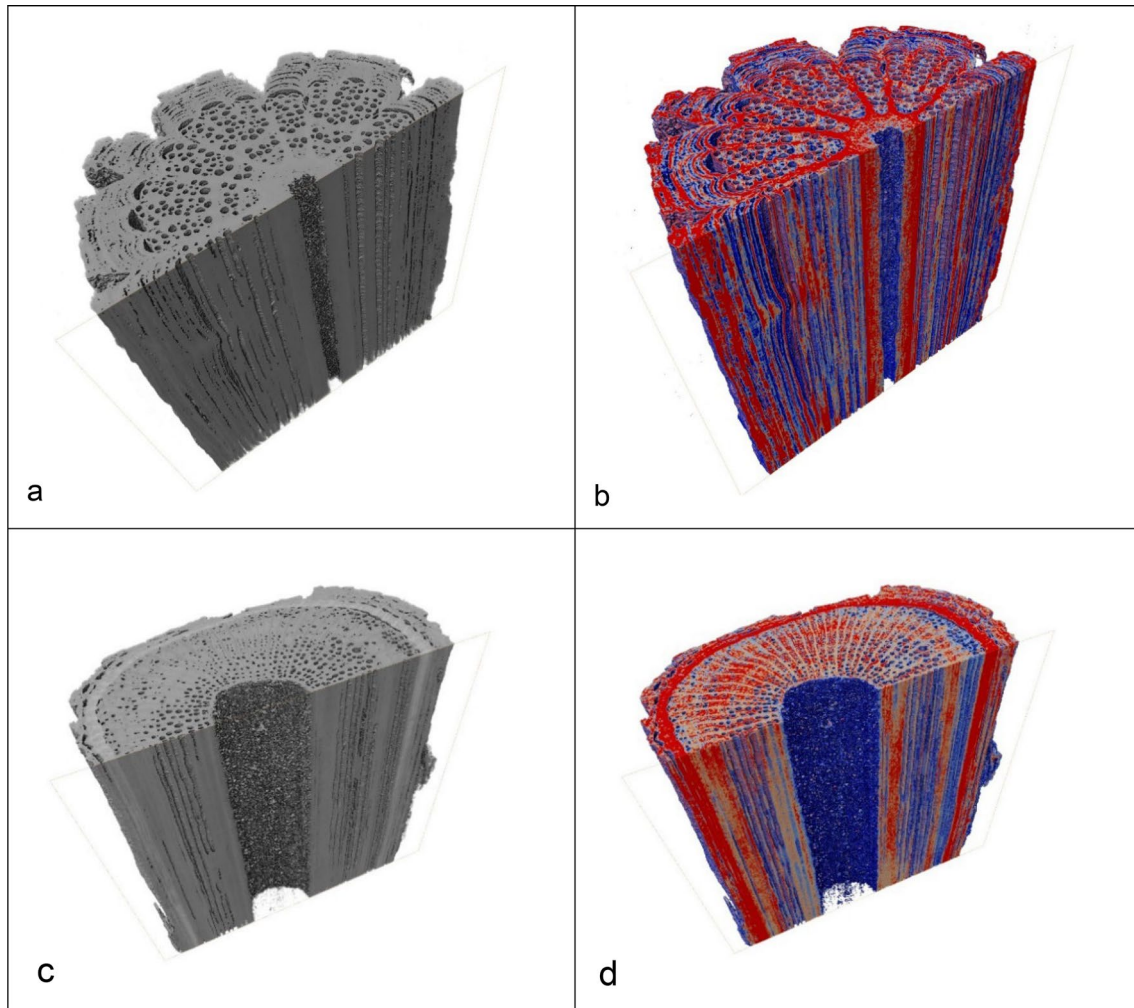


Fig. 8 Micro-CT half-volume rendering of *Clematis vitalba* in volume rendering with grey values (a), and coloured representation of the same sections using a continuous colour scale for easy comparison with the histological sections in Fig. 6b. Same for *Vitis vinifera*

in (c) and (d). Red colour represents regions of relative high density, blue colour represents regions of relative intermediate density and no colour represents regions of relatively low density (voids)

of *V. vinifera* specimens however failed close to the gripping area, either due to nodes located there (Fig. 11d), due to material defects (Fig. 11f), or due to additional bending moment at the area due to the specimen curvature (Fig. 11e). For these reasons, the estimated ultimate stress values were considered as indicative strength values of the examined materials.

Representative stress–strain curves for both specimen types are presented in Fig. 12. It appears that *V. vinifera* specimen is stiffer and stronger than *C. vitalba* specimen.

This contrasting result was confirmed with measures on a series of specimens (Table 1). *Vitis vinifera* has an average stiffness of 2.62 ± 1.51 GPa and an average strength of 37.77 ± 8.89 MPa, while *C. vitalba* is around 30% less stiff with an average stiffness of 1.81 ± 0.88 GPa and around 50% less strong reaching an average strength of

18.50 ± 3.03 MPa. Although cannot be directly compared these values are in the range of other published results for plants, e.g. Rowe et al. (2004) although most of the previous works were performing flexural experiments instead of tensile strength experiments and a number of them used specimens on their natural hydrated state, instead of dried as in this study. The higher mechanical properties of *V. vinifera* as compared to *C. vitalba* can be explained by the smaller percentage of voids in the volume in combination with the higher proportion of higher density material in the *V. vinifera* (ca. 61%) compared to the corresponding in the *C. vitalba* (ca. 26%) as presented in Sect. “CT analysis of microstructures” and Fig. 9.

For both plants, the variation was more on the Young modulus (coefficients of variation CV: 0.49–0.58) and less on the strength (CV: 0.16–0.24). Furthermore, it

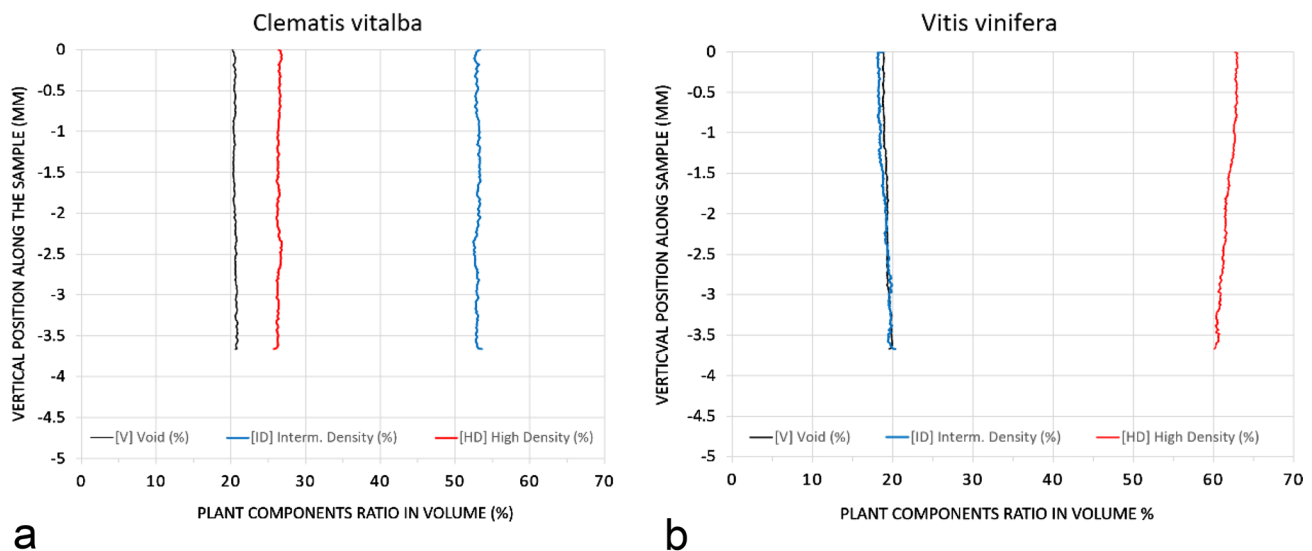


Fig. 9 Volumes of three regions of different density (HD, ID and V) in a representative sample volume of 482.8 mm³ and 327.2 mm³ in *Clematis vitalba* (a) and *Vitis vinifera* (b), respectively, in function of the vertical position along the sample

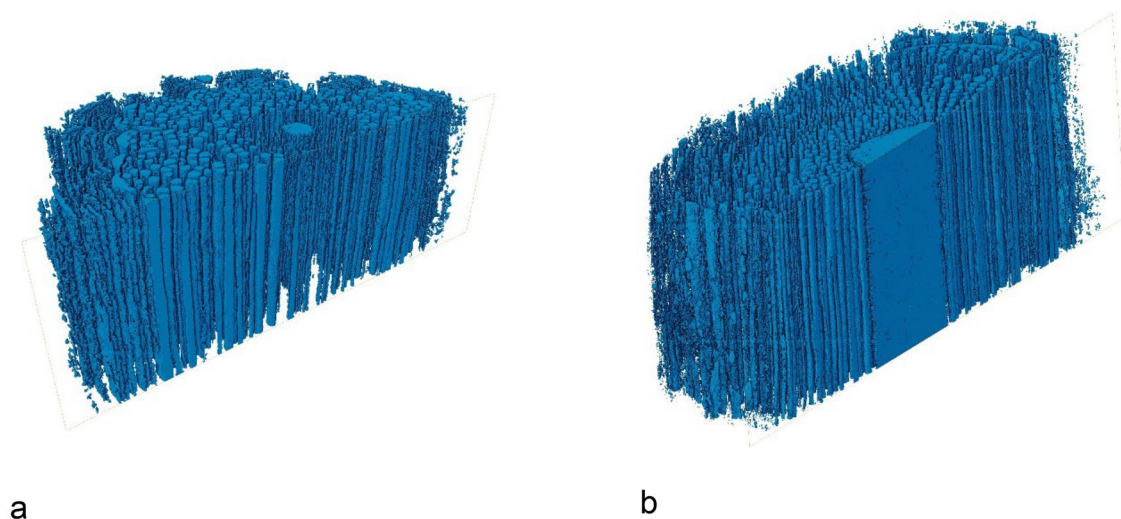


Fig. 10 Micro-CT half-volume representation of the segmented void regions (V) in *Clematis vitalba* (a) and *Vitis vinifera* (b)

was observed that the stiffer specimens tended also to be stronger (Fig. 13), without however any correlation between the two properties.

Both strength and stiffness seem to be independent of the plant's cross section as presented in Fig. 14. A similar observation was reported in Gallenmüller et al. (2001), indicating that free-standing plants show a nearly constant structural Young's modulus, while their flexural stiffness (EI) is increasing proportionally with the sectional moment of inertia. Therefore, such plants develop a geometrical flexural stiffness correlated to their dimensions—higher at the roots where the plant is thicker, and lower at the upper level where the plant is thinner. Both studied lianas

are non-self-supporting plants but it has been demonstrated that the mechanical properties can change importantly during the development of the plants. Like many lianas, young individual plants of *C. vitalba* show relatively high values of structural Young's modulus and older wider stems show a significant drop by up to 95%, while flexural stiffness is increasing linearly with axial second moment of area of the stem (Rowe et al. 2004; Schweingruber 1983). This can be probably explained by the change of growth strategy of such climbing plants, where young axes are relatively stiff (due to primary fibre bundles) to reach supports and older stages become highly compliant (formation of compliant wood) to adapt to movements in the canopy. This pattern could not be



Fig. 11 Typical examples of failure modes of *Clematis vitalba* (C) and *Vitis vinifera* (V) specimens. **a** C1, **b** C2, **c** C10, **d** V7, **e** V14, **f** V19

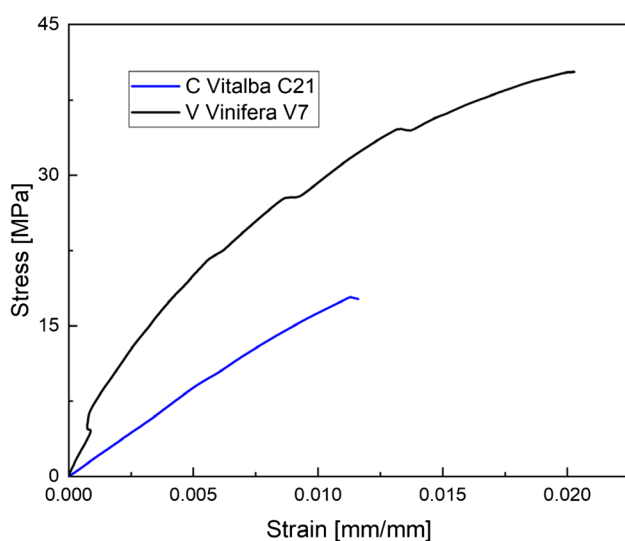


Fig. 12 Typical stress–strain curves of the two plants species *Clematis vitalba* and *Vitis vinifera*

observed with the data presented in this work, which did not comprise the very young stems of *C. vitalba*. This contrasted mechanical behaviour aligns with the functional perspective by the difference in fructification of both species. The higher flexural resistance of *V. vinifera* is necessary to support the heavy bunches of fruits, while *C. vitalba* has remarkably light dried fruits called achenes.

Numerical modelling

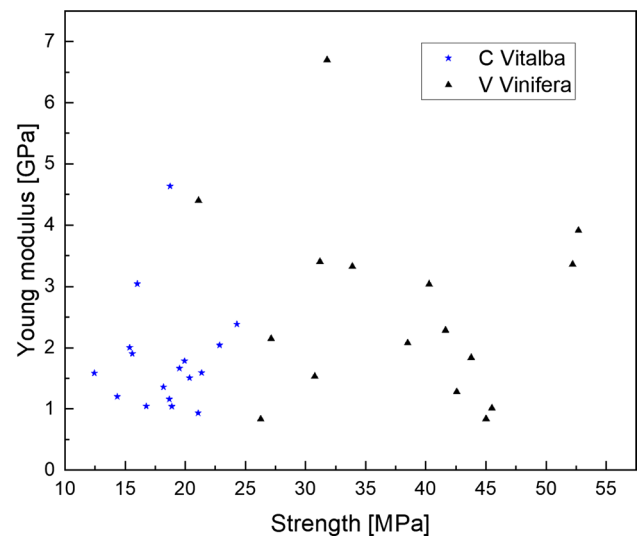
Two ABAQUS models were derived by extrusion of homogeneous solids based on the sketches of the two plant species derived from the micro-CT images as shown in Fig. 5. Cyclic symmetry was used as explained in section “[numerical modelling](#)”, and therefore, a quarter section was employed for the *C. vitalba* and a half section for *V. vinifera*. Although the examined plants were not symmetric the model was. In the model, the bottom part is fixed, while the upper part was subjected to tension at a constant displacement rate of 1 mm/min for a total time of 300–360 s. The simulation was not time dependent. A tetrahedral mesh was generated for both plant sections (Fig. 15), with a 1-mm spacing along the plant

Table 1 Summary of the mechanical experimental results of tensile strength and stiffness on *Clematis vitalba* (C1–C27 specimens) and *Vitis vinifera* (V1–V23 specimens)

Specimen ID	Cross-sectional diameter (mm)	Tensile strength (MPa)	Stiffness—Young modulus (GPa)
C7	5.6	22.86	2.04
C20	5.9	18.75	4.63
C21	5.9	19.95	1.78
C26	5.9	15.6	1.9
C23	6	12.44	1.58
C22	6.1	18.2	1.36
C25	6.1	18.68	1.16
C27	6.9	16.76	1.04
C19	7.6	24.29	2.38
C6	9.3	14.35	1.2
C1	10	21.07	0.93
C18	10	16.02	3.04
C10	10.1	15.38	2
C3	11.4	19.52	1.66
C16	11.4	20.36	1.5
C2	11.5	18.89	1.04
C24	11.5	21.36	1.59
Average		18.50	1.81
Standard deviation		3.03	0.88
V10	5.3	42.57	1.28
V13	5.3	52.21	3.36
V14	5.5	52.7	3.91
V16	5.5	31.8	6.7
V15	5.9	31.2	3.4
V18	6.5	26.28	0.83
V2	7	43.78	1.84
V12	7.7	33.89	3.32
V19	8.6	45.01	0.84
V1	9.2	30.76	1.53
V7	10	40.28	3.04
V17	10	38.5	2.08
V21	10	41.65	2.29
V23	10.5	45.5	1.01
V20	10.9	21.1	4.4
V22	11.8	27.15	2.15
Average		37.77	2.62
Standard deviation		8.89	1.51

Various failure modes were observed for both wood species, and the derived strength values are considered as indicative for comparison

length and a refined precision around delicate void regions. The mesh of the *C. vitalba* plant model contained 582'845 elements in total, which makes 6'857 elements every 1 mm along the plant. The simulation time was approximately 60 min. The mesh of the *V. vinifera* is composed by

**Fig. 13** Relationship between strength and Young modulus of both species *Clematis vitalba* and *Vitis vinifera*

1'336'480 linear hexahedral elements with 1'434'834 nodes, and the simulation time was approximately 160 min.

Preliminary checks were performed to confirm the uniformity of the stress along the plants stem and at any cross section. Indicative photos are presented in Fig. 16 confirming the uniformity along the plant axis for the *C. vitalba* model. The boundary effects are perceptible until ca. 15 mm after the tension grip and before the fixed boundary; however, all along the specimen axis in between these boundaries the normal stress remains constant. The same holds true for *V. vinifera*.

The stress at each cross section in between these boundaries was also constant, Fig. 17 shows selectively the results for the *V. vinifera* model, although similar results were also obtained from the *C. vitalba* model. The stress in Fig. 17 slightly fluctuates, however differences not more than 3% can be calculated (min stress 217.6 MPa, max stress 223.4 MPa).

Discussion

2D comparison of imaging methods

A comparison of the 2D cross sections shown in Figs. 6 and 7, generated from microtome sections and micro-CT scanning, respectively, shows that similar internal structures can be visualized with both methods and for both analysed plant species. Nevertheless, the staining of the microtome sections with Astrablue and Safranin results in a differentiation of tissue types according to their chemical composition, namely the presence or absence of lignin (cf. Fig. 6). For the micro-CT slices, the image segmentation

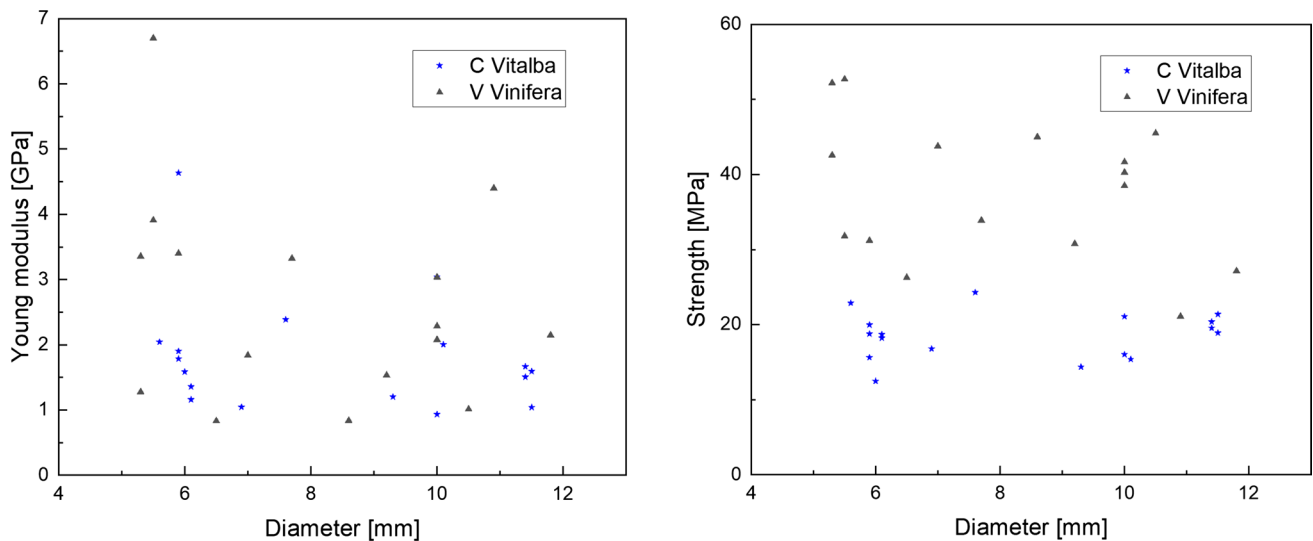


Fig. 14 Correlation between mechanical properties (Young modulus and strength) and diameter of the stems

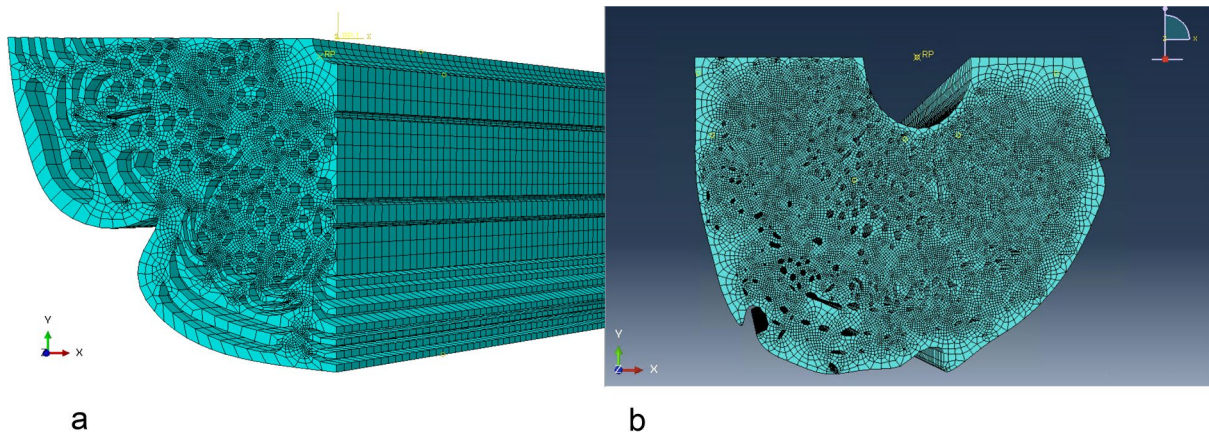


Fig. 15 Mesh of numerical models for both plant structures. *Clematis vitalba* (a), *Vitis vinifera* (b)

is based on the X-ray attenuation coefficient of the different tissue types and represents their variations in density. Also, in this work, voids smaller than the image resolution (estimated to 3–4 times the voxel size, i.e. around 30 to 40 microns) are not captured, and on a small scale, the structure is imaged as a homogeneous material, meaning that individual cell walls are not distinguished. The staining of the microtome sections, however, results in the visualization of only the cell walls, which can be discerned separately with a microscope. Comparing the results of the two colouring methods in *C. vitalba*, the lignified tissues appear in general to coincide well with the denser parts of the cross section (coloured red in both images); however, parts of the xylem that are lignified according to Fig. 6 are blue (relatively low density) in the micro-CT representation (Fig. 7), and the non-lignified phloem is not

properly captured at all in Fig. 7 (appears as void—V). In *V. vinifera*, the lignified tissue and high-density tissues do not coincide well. The medullary rays are shown in blue (low density) in the micro-CT section even though they are lignified, and the phloem appears as the zone of highest density (red) but is made up of lignified as well as non-lignified cells (blue in Fig. 6), which is not very well represented in the micro-CT scan. The xylem region directly adjacent to the phloem appears of lower density and borders a denser xylem region towards the centre of the section. This can be observed on the micro-CT scan through the differentiation between blue and red colour (Fig. 7) and in the microtome section by variation in densities (visual) of the individual cells, and therefore a variation in the intensity of red colour (Fig. 7). These insights suggest that the image segmentation based on the material density

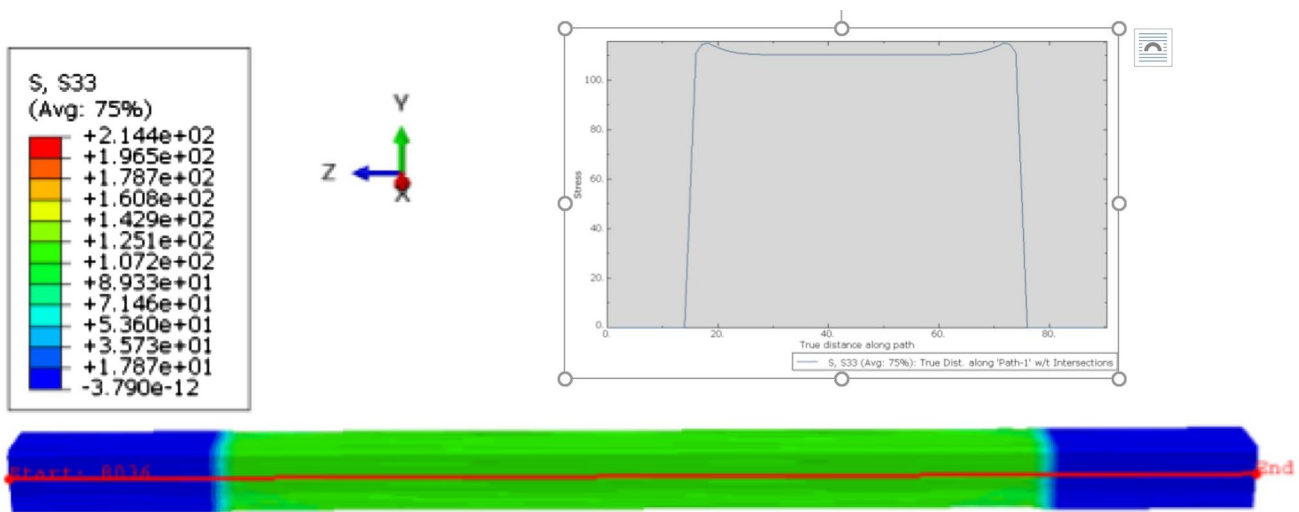


Fig. 16 FE model results. Stress uniformity along the specimen axis—*Clematis vitalba*

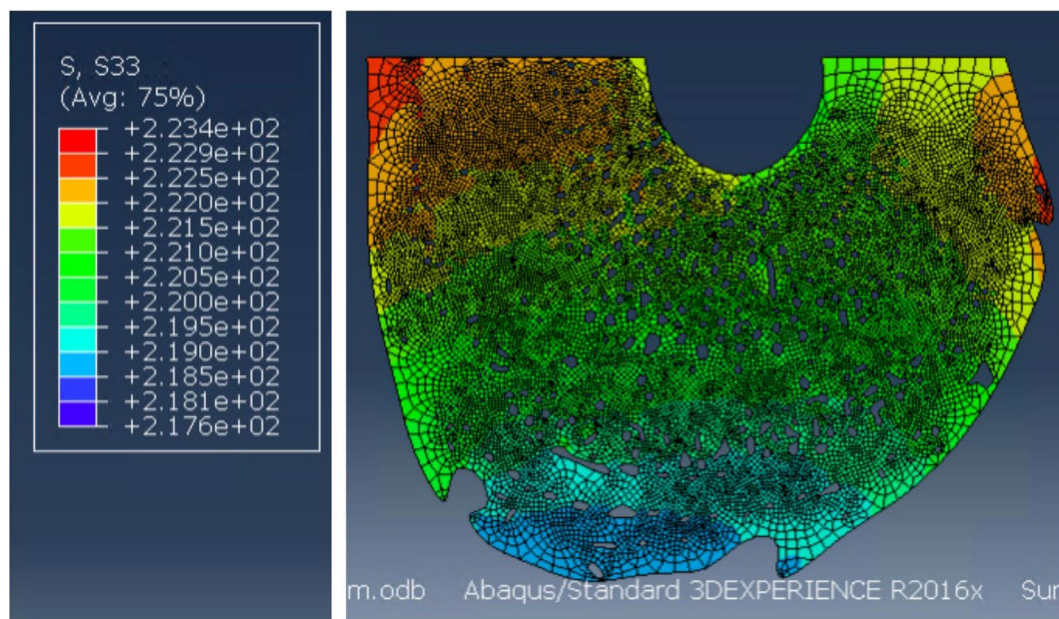


Fig. 17 FE model results. Stress uniformity through the cross section—*Vitis vinifera*

and with the chosen threshold value does not entirely coincide with the differentiation of materials according to their chemical composition. From a plant mechanical perspective, the fibre cells with lignified secondary cell walls are most important for the structural support. These are coloured red in the micro-CT images and are located in *C. vitalba* along the medullary rays and surrounding the phloem, and in *V. vinifera*, they are associated with the xylem and the phloem. The parts appearing blue in the micro-CT images are associated with the xylem and the periderm in *C. vitalba*, and in *V. vinifera*, they are associated with the medullary rays, the outer part of the xylem

and the periderm. These are all cells of parenchymatic nature, sieve elements in the phloem or less dense fibre cells which are of minor structural importance. Therefore, we suggest the employed segmentation of micro-CT images to discern between the stem components with mechanical importance and those without or with minor mechanical importance.

From a methodological perspective, this means that the conventional staining method and the image segmentation of micro-CT scans do not provide exactly similar information in relation to plant's functionality but complement each other. The stained microtome sections can be used to evaluate the

coincidence of the micro-CT-based density differentiation with the differentiation of tissue types based on their biological function, which can partially be inferred through the knowledge about the chemical composition of the cell walls. In addition, the microscopic view of the microtome sections allows for a better distinction of individual cells and small voids, especially for larger samples for which the resolution of micro-CT is not high enough.

We also suggest that although micro-CT provides a simpler structural model than that provided by histological sections, this model is sufficiently detailed to highlight the differences in mechanical behaviour as discussed below.

In this section we have compared the two imaging methods in 2D but a major advantage of micro-CT is the ability to determine the continuity of plant pore structures in 3D in order to infer their functional properties and use them as input when modelling their mechanical behaviour.

Simulation versus experimental results

The simulation for the force displacement was successful for both species. A perfectly elastic behaviour is observed as expected for the linear analysis. For *Clematis vitalba*, the force reaches 5.13 kN for a displacement of 5 mm, while for the *Vitis vinifera*, the force reaches 5.3 kN for 5 mm of displacement. These values correspond to stiffness of 1.4–1.9 GPa (*Clematis* with voids, and without voids) and 2.2 GPa (*Vitis*) and are similar to the experimentally derived values of 1.81 ± 0.88 GPa and 2.62 ± 1.51 GPa accordingly (See Table 1). The FEA simulation of the tension experiment performed on both plant species was successful showing that the extrusion of a simplified section assuming a single homogeneous material is a good approximation. Although by extruding a single section the variability of the cross sections along the stem is not considered, this did not seem to have a significant effect on the results.

Conclusions

In this study, detailed imaging of the internal structure of two types of lianas was carried out by coupling X-ray micro-CT and anatomical cross-sectional observation. The comparison of these two methods shows that their contributions are different but coherent and complementary. The comprehensive material characterization obtained by these two methods was successfully used to derive a FE model of the plants' structure and analyse their mechanical performance. The classical method of anatomical cross sections allows the identification of the structures of the lianas in 2D with great precision and allows the identification of the

lignified parts, supposedly more resistant mechanically, of these structures. Micro-CT provides a full 3D model of the structure, admittedly less detailed but providing the spatial distribution of density contrasts which can be important in the mechanical properties of the plant. The derivation of the 3D model based on the micro-CT results facilitates the characterization of the structural heterogeneity in a given volume of the plant, e.g. continuity of the porous structure, and allows the consideration of this internal material structure by the FE modelling, offering this way an accurate analysis of the plant's mechanical behaviour, which is practically not achievable on the basis of 2D thin slices.

The relationships between the 3D structural model and the results of mechanical tensile tests on these two liana species are discussed and show consistent trends. In particular, the stress–strain curve shows that the *V. vinifera* specimen is stiffer and stronger than that of *C. vitalba* and, based on the 3D structural model, the higher mechanical properties of *V. vinifera*, compared to *C. vitalba*, can be logically explained by the lower percentage of voids (essentially vessels) in combination with a higher proportion of high-density material in *V. vinifera* than in *C. vitalba*.

The structures identified on the basis of the 3D model for each of the two liana species are discretized and used, in a simplified manner, to model the mechanical behaviour of the two lianas and to compare the simulation results which take into account not only the volume fraction of the different components but also the spatial distribution of these components within the specimen studied.

The proposed methodological approach opens new perspectives to better understand the mechanical behaviour of the complex structure of plants and to draw inspiration from it in structural engineering.

Acknowledgements The authors would like to thank Mr. Gary Perrenoud for realizing the CT scans and for preparing the mechanical tests. They also thank Mr. Arielle Forni and Mr. Lucas Mathevet for carrying out the mechanical tests.

Author contributions CK selected the plants, analysed the microscopy and CT data and took part to the redaction. PT analysed the CT data and took part to the redaction. AB selected the plants, analysed the microscopy data and took part to the redaction. OM realized the mechanical modelling and took part to the redaction. FS realized the plants thin slices and analysed the microscopy data. APV analysed the mechanical tests and modelling and took part to the article redaction.

Funding Open access funding provided by EPFL Lausanne. This research work was partially financed by a grant (Exploratory grant) of the ENAC School of the EPFL.

Availability of data and materials The datasets used and/or analysed during the current study are available from the corresponding author on reasonable request.

Declarations

Conflict of interest The authors declare that they have no competing interest.

Ethical approval No applicable.

Open Access This article is licensed under a Creative Commons Attribution 4.0 International License, which permits use, sharing, adaptation, distribution and reproduction in any medium or format, as long as you give appropriate credit to the original author(s) and the source, provide a link to the Creative Commons licence, and indicate if changes were made. The images or other third party material in this article are included in the article's Creative Commons licence, unless indicated otherwise in a credit line to the material. If material is not included in the article's Creative Commons licence and your intended use is not permitted by statutory regulation or exceeds the permitted use, you will need to obtain permission directly from the copyright holder. To view a copy of this licence, visit <http://creativecommons.org/licenses/by/4.0/>.

References

- Baley C, Goudenhooft C, Gibaud M, Bourmaud A (2018) Flax stems: from a specific architecture to an instructive model for bioinspired composite structures. *Bioinsp Biomimet* 13:026007. <https://doi.org/10.1088/1748-3190/aaa6b7>
- Brodersen CR, Roddy AB (2016) New frontiers in the three-dimensional visualization of plant structure and function. *Amer J Bot* 103:184–188. <https://doi.org/10.3732/ajb.1500532>
- Brodersen CR, Chatelet DS, Shackel KA, Matthews MA, McElrone AJ (2013) Xylem vessel relays contribute to radial connectivity in grapevine stems (*Vitis vinifera* and *V. arizonica*; Vitaceae). *Amer J Bot* 100:314–321. <https://doi.org/10.3732/ajb.1100606>
- Calo CM, Rizzutto MA, Carmello-Guerreiro SM, Dias CSB, Watling J, Shock MP, Zimpel CA, Furquim LP, Pugliese F, Neves EG (2020) A correlation analysis of light microscopy and x-ray MicroCT imaging methods applied to archaeological plant remains' morphological attributes visualization. *Sci Rep* 10:1–15. <https://doi.org/10.1038/s41598-020-71726-z>
- Competence Network Biomimetics - Technical Plant Stem. <https://www.kompetenznetz-biomimetik.de/technischer-pflanzenhalm/>
- Dixon PG, Ahvenainen P, Aijazi AN, Chen SH, Lin S, Augusciak PK, Borrega M, Svedström K, Gibson LJ (2015) Comparison of the structure and flexural properties of Moso, Guadua and Tre Gai Bamboo. *Constr Build Mater* 90:11–17. <https://doi.org/10.1016/j.conbuildmat.2015.04.042>
- Dixon PG, Muth JT, Xiao X, Skylar-Scott MA, Lewis JA, Gibson LJ (2018) 3D printed structures for modeling the young's modulus of bamboo parenchyma. *Acta Biomater* 68:90–98. <https://doi.org/10.1016/j.actbio.2017.12.036>
- Duncan KE, Czymmek KJ, Jiang N, Thies AC, Topp CN (2022) X-ray microscopy enables multiscale high-resolution 3D imaging of plant cells, tissues, and organs. *PL Physiol* 188:831–845. <https://doi.org/10.1093/plphys/kiab405>
- Ennos AR (1993) The mechanics of the flower stem of the sedge *Carex acutiformis*. *Ann Bot (Oxford)* 72:123–127
- Forell V, Greg DR, Lee SY, Cook DD (2015) Preventing lodging in bioenergy crops: a biomechanical analysis of maize stalks suggests a new approach. *J Exp Bot* 66:4367–4371. <https://doi.org/10.1093/jxb/erv108>
- Gallenmüller F, Müller U, Rowe N, Speck T (2001) The growth form of croton Pullei (*Euphorbiaceae*) - functional morphology and biomechanics of a Neotropical liana. *PL Biol* 3:50–61
- Gao Y, Yang Z, Wang G, Sun J, Zhang X (2020) Discerning the difference between lumens and scalariform perforation plates in impeding water flow in single xylem vessels and vessel networks in cotton. *Frontiers Pl Sci* 11:1–12. <https://doi.org/10.3389/fpls.2020.00246>
- Gärtner H, Fritz H, Schweingruber (2013) Microscopic preparation techniques for plant stem analysis. Verlag Kessel, Oberwinter
- Green DW, Winandy JE, Kretschmann DE (1999) Mechanical properties of wood. In: Forest Products Laboratory (eds) Wood handbook: wood as an engineering material. General Technical Report FPL ; GTR-113. USDA Forest Service, Madison, pp 4.1–4.45
- He J, Lyu R, Luo Y, Xiao J, Xie L, Wen J, Li W, Pei L, Cheng J (2022) A phylotranscriptome study using silica gel-dried leaf tissues produces an updated robust phylogeny of Ranunculaceae. *Molec Phylogen Evol* 174:107545. <https://doi.org/10.1016/j.ympev.2022.107545>
- Hoffmann B, Chabbert B, Monties B, Speck T (2003) Mechanical, chemical and X-ray analysis of wood in the two tropical Lianas *Bauhinia guianensis* and *Condylocarpon guianense*: variations during ontogeny. *Planta* 217:32–40
- Holmlund HI, Pratt RB, Jacobsen AL, Davis SD, Pittermann J (2019) High-resolution computed tomography reveals dynamics of desiccation and rehydration in fern petioles of a desiccation-tolerant fern. *New Phytol* 224:97–105. <https://doi.org/10.1111/nph.16067>
- Isnard S, Speck T, Rowe NP (2003) Mechanical architecture and development in clematis: implications for canalised evolution of growth forms. *New Phytol* 158:543–559
- Jellum MD (1962) Relationships between lodging resistance and certain culm characters in oats. *Crop Sci* 2:263–267
- Kaack K, Schwarz K-U, Brander PE (2003) Variation in morphology, anatomy and chemistry of stems of miscanthus genotypes differing in mechanical properties. *Industr Crops Prod* 17:131–142
- Koddenberg T, Militz H (2018) Morphological imaging and quantification of axial xylem tissue in *Fraxinus excelsior* L. through X-ray micro-computed tomography. *Micron* 111:28–35. <https://doi.org/10.1016/j.micron.2018.05.004>
- Lehmann H, Schulz D (1976) Die pflanzenzelle struktur und funktion. Ulmer, Stuttgart
- Li X, Sylvain D, José TRM, Eric B, Régis B, Hervé C, Steven J, Andrew K, Laurent L, Nicolas L, Nicolas MS, Brendan B (2020) Lack of vulnerability segmentation in four angiosperm tree species: evidence from direct X-ray microtomography observation. *Ann Forest Sci* 77:1–12. <https://doi.org/10.1007/s13595-020-00944-2>
- Liu XQ, Ickert-Bond SM, Nie ZL, Zhou Z, Chen LQ, Wen J (2016) Phylogeny of the *Ampelocissus-Vitis* clade in Vitaceae supports the New World origin of the grape genus. *Molec Phylogen Evol* 95:217–228. <https://doi.org/10.1016/j.ympev.2015.10.013>
- Maire E, Withers PJ (2014) Quantitative X-ray tomography. *Int Mater Rev* 59:1–43. <https://doi.org/10.1179/1743280413Y.0000000023>
- Masselter T, Speck T (2011) Biomimetic fiber-reinforced compound materials. In: Cavrak M (ed) Advances in biomimetics. InTech, Rijeka, pp 185–210
- Mayo SC, Chen F, Evans R (2010) Micron-scale 3D imaging of wood and plant microstructure using high-resolution X-ray phase-contrast microtomography. *J Struct Biol* 171:182–188. <https://doi.org/10.1016/j.jsb.2010.04.001>
- Milwich M, Speck T, Speck O, Stegmaier T, Planck H (2006) Biomimetics and technical textiles: solving engineering problems with the help of nature's wisdom. *Amer J Bot* 93:1455–1465
- Moshtaghin AF, Franke S, Keller T, Vassilopoulos AP (2016) The statistical variability and length effects in the tensile transverse

- behavior of clear timber. In WCTE 2016 - World Conference on Timber Engineering
- Mylo MD, Hofmann M, Delp A, Scholz R, Walther F, Speck T, Speck O (2021) Advances on the visualization of the internal structures of the European mistletoe: 3D reconstruction using microtomography. *Frontiers Pl Sci* 12:1–13. <https://doi.org/10.3389/fpls.2021.715711>
- Niklas KJ, Spatz HC, Vincent J (2006) Plant biomechanics: an overview and prospectus. *Amer J Bot* 93:1369–1378
- Obataya E, Kitin P, Yamauchi H (2007) Bending characteristics of bamboo (*Phyllostachys pubescens*) with respect to its fiber-foam composite structure. *Wood Sci Technol* 41:385–400. <https://doi.org/10.1007/s00226-007-0127-8>
- Pajor R, Fleming A, Osborne CP, Rolfe SA, Sturrock CJ, Mooney SJ (2013) Seeing space: visualization and quantification of plant leaf structure using X-ray micro-computed tomography. *J Exp Bot* 64:385–390. <https://doi.org/10.1093/jxb/ers392>
- Palombini FL, Kindlein W Jr, de Oliveira BF, de Araujo Mariath JE (2016) Bionics and DESIGN: 3D microstructural characterization and numerical analysis of bamboo based on X-ray microtomography. *Mater Charact* 120:357–68. <https://doi.org/10.1016/j.matchar.2016.09.022>
- Palombini FL, Lautert EL, Mariath JEDA, de Oliveira BF (2020) Combining numerical models and discretizing methods in the analysis of bamboo parenchyma using finite element analysis based on X-ray microtomography. *Wood Sci Technol* 54:161–186. <https://doi.org/10.1007/s00226-019-01146-4>
- Palombini FL, Nogueira FM, Kindlein W, Paciornik S, Mariath JE, de Oliveira BF (2019) Biomimetic systems and design in the 3D characterization of the complex vascular system of bamboo node based on X-ray microtomography and finite element analysis. *J Mater Res* 35:842–854. <https://doi.org/10.1557/jmr.2019.117>
- Rowe N, Isnard S, Speck T (2004) Diversity of mechanical architectures in climbing plants: an evolutionary perspective. *J Pl Growth Regulat* 23:108–128. <https://doi.org/10.1007/s00344-004-0044-0>
- Rüggeberg M, Speck T, Paris O, Lapierre C, Pollet B, Koch G, Burgert I (2008) Stiffness gradients in vascular bundles of the palm *Washingtonia robusta*. *Proc Roy Soc B Biol Sci* 275:2221–2229. <https://doi.org/10.1098/rspb.2008.0531>
- Schweingruber FH, Börner A (2018) The plant stem. A microscopic aspect. Springer, Cham
- Schweingruber, Fritz H (1983) Schweingruber Microscopic wood anatomy. *Folia Geobot Phytotax* 18:447–448. <https://doi.org/10.1007/BF02857272>
- Speck T, Burgert I (2011) Plant stems: functional design and mechanics. *Annual Rev Mater Res* 41:169–193. <https://doi.org/10.1146/annurev-matsci-062910-100425>
- Torregrosa L, Carbonneau A, Kelner JJ (2021) The shoot system architecture of *Vitis vinifera* ssp. *sativa*. *Sci Hortic* 288:110404. <https://doi.org/10.1016/j.scienta.2021.110404>
- Toumpanaki E, Shah DU, Eichhorn SJ (2021) Beyond what meets the eye: imaging and imagining wood mechanical-structural properties. *Advanced Mater* 33:1–22
- Wang W, Lin L, Xiang XG, Ortiz Rdel C, Liu Y, Xiang KL, Yu SX, Xing YW, Chen ZD (2016) The rise of angiosperm-dominated *Herbaceous floras*: insights from Ranunculaceae. *Sci Rep* 6:6–13. <https://doi.org/10.1038/srep27259>
- Wen J, Xiong Z, Nie ZL, Mao L, Zhu Y, Kan XZ, Ickert-Bond SM, Gerrath J, Zimmer EA, Fang XD (2013) Transcriptome sequences resolve deep relationships of the grape family. *PLoS ONE* 8:1–9. <https://doi.org/10.1371/journal.pone.0074394>

Publisher's Note Springer Nature remains neutral with regard to jurisdictional claims in published maps and institutional affiliations.